Res. Rep. Fac. Eng. Mie Univ., Vol. 21, pp. 11−25 (1996)

Original Paper

Influence of Microstructure on Embrittlement and Loss of Ductility in HAZ of 2 1/4Cr-1Mo Steel

Koreaki TAMAKI, Hiroshi KAWAKAMI, Jippei SUZUKI
Michita MIZUNO and Toshimasa NIINOMI
(Department of Mechanical Engineering)

(Received September 13, 1996)

Abstract

The low ductility creep fracture (LDCF) and the temper embrittlement (TE) arised in the heat affected zone (HAZ) when the welded constructions of Cr-Mo steels were used at their service temperatures around 800K. The former was reproduced in the laboratory by the creep-rupture test at the temperature range of 775K to 875K on the synthetic HAZ specimens. The latter was reproduced by the impact test on the specimens tempered at those temperatures. Four types of LDCF (LDCF 1 to 4) and four types of temper embrittlement (TE 1 to 4) were recognized. LDCF 1, 2, 3 and 4, respectively appear in the same time-temperature ranges as those in which TE 1, 2, 3 and 4 arise. Common metallurgical causes of the LDCF and TE were discussed. LDCF 1, 2 and TE 1, 2, which arise in the short-term range, will be induced both by the loss of ductility in ferrite matrix and the segregation of impurities in grain boundaries. LDCF 3 and TE 3, which arises in the long-term range, will be induced by the segregation of impurities in grain boundaries. LDCF 4 and TE 4, which appears in the high temperature range, will be brought about by the coarsening of carbide particles in ferrite matrix.

Key words: Cr-Mo steels, heat affected zone, low-ductility creep fracture, temper embrittlement, loss of ductility, segregation of impurities, coarsening of carbide.

1. Introduction

The low ductility creep fracture (LDCF)[1–4] and the temper embrittlement (TE)[5–8] have been occasionally observed in the heat affected zone (HAZ) of Cr–Mo steels when the welded constructions, such as boilers and pressure vessels were reheated in certain temperature range around 800K. The former occurs in HAZ at the time when the welded constructions were used at their service temperatures. The latter is detected as the rise of transition temperature in the HAZ which was caused by the long–term services. The LDCF was reproduced in the laboratory by the creep–rupture test at the temperature range of 775K to 875K on the synthetic HAZ specimens. The TE was reproduced by the impact test on the specimens tempered at those temperatures.

The major metallurgical factors to cause those phenomena will be common in some extent for both of them. The relations between the LDCF and the TE and following metallurgical factors were discussed in this report. (1)precipitation and growth of carbide particles, (2)segregation of impurity elements.

2. General features of low ductility creep fracture

2.1 Experimental procedure

2 1/4Cr–1Mo steel (A) of the chemical composition shown in Table 1 was used for the experiment of LDCF. The microstructure of HAZ, which was given by arc welding with the heat input of 17.3kJ/cm, was reproduced in a steel bar by using a weld–thermal–cycle simulator[4]. A notched specimen shown in Fig.1 was used for the creep rupture test. An uniform microstructure was produced in its center portion of 20mm in length. The test temperatures were 775, 825, 850 and 875K; the maximum fractuation from each temperature was 5K. The specimen was heated to each given temperature in 1 hour, kept 1 hour at this temperature and then a stress in the range of 200 to 800MPa was loaded.

Table 1 Chemical compotiton of 2 1/4Cr–1Mo steel, wt%.

	C	Si	Mn	P	S	Cr	Mo	Cu	Ni	As	Al_{sol}	N
Steel (A)	**0.15**	**0.12**	**0.52**	**0.004**	**0.001**	**2.40**	**1.05**	**0.01**	**0.18**	**0.002**	**0.015**	**0.0059**
Steel (B)	**0.14**	**0.16**	**0.56**	**0.006**	**0.002**	**2.17**	**0.90**	**0.01**	**0.13**	**0.004**	**0.017**	**0.0032**

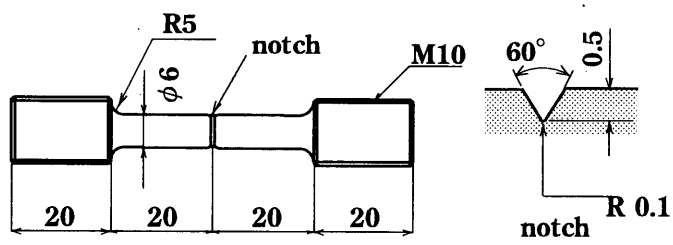

Fig.1 Specimen for creep–rupture test.

2.2 Relations among stress, time to fracture and ductility

The diagram of the stress and the time to fracture at the test temperature of 825K is shown by the mark ○ in Fig.2(a). The data of base metal specimens are shown by the mark ●. In the higher stress revel, the time to fracture is larger for the HAZ specimen than for the base metal, but their situation is reversed in the lower stress revel, these results are similar to those in the previous researches [1–3]. Nevertheless, the time to fracture of HAZ specimen does not so

much differ from that of base metal.

The reduction in area of each specimen was plotted against the time to fracture as shown in Fig.2(b). Comparing with the base metal specimen, the reduction in area is very small (smaller than 20%) for all the HAZ specimens. However, it increases a little when the time exceeds a critical time period of t_r.

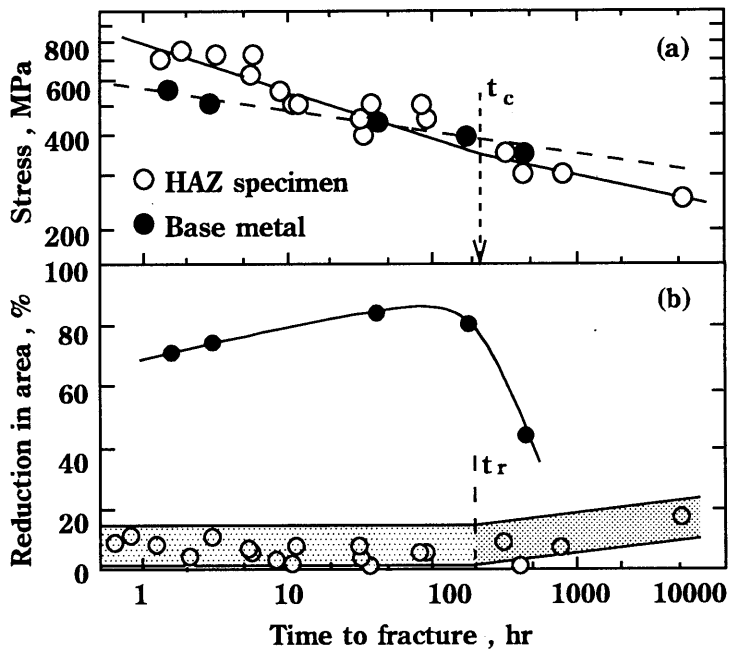

Fig.2 Results of creep–rupture test of HAZ and base metal specimens; test temperature 825K.

2.3 Classification of fracture mode

Fracture surfaces of specimen were observed by an SEM with magnifications of 100 to 500. Fracture modes of all the specimens were classified by their appearances into four major groups. Type I (Fig.3(a)) exhibits a typical intergranular fracture which occurs along the grain boundaries of prior-austenite. The surfaces of each crystal grain are flat and smooth, and edges of each grain are very sharp. Type II (Fig.3(b)) is produced along the grain boundaries of prior-austenite as the case of type I, but it differs from that in the following special features: (1)each crystal grain is deformed in some extent, (2)a wavy pattern is observed on some surfaces of a grain, (3)some cracks run into the crystal grains.

Type III belongs to the ductile fracture of transgranular mode. It is observed around the center portion of the specimen where the final fracture occured. It includes both the typical dimple mode (Fig.3(c)), and a ductile fracture of which the facets are large and irregular in size. Type IV (Fig.3(d)) belongs to the brittle fracture of transgranular mode. It is observed in the center portion of the specimen fractured after 4000 hours at the temperature as high as 875K. A flat and smooth surface with little deformation in ferrite grains of this type suggests that it may belong to the cleavage fracture.

2.4 Influence of time to fracture on fracture type

The area of each type of fracture was measured on each specimen, and the fraction of

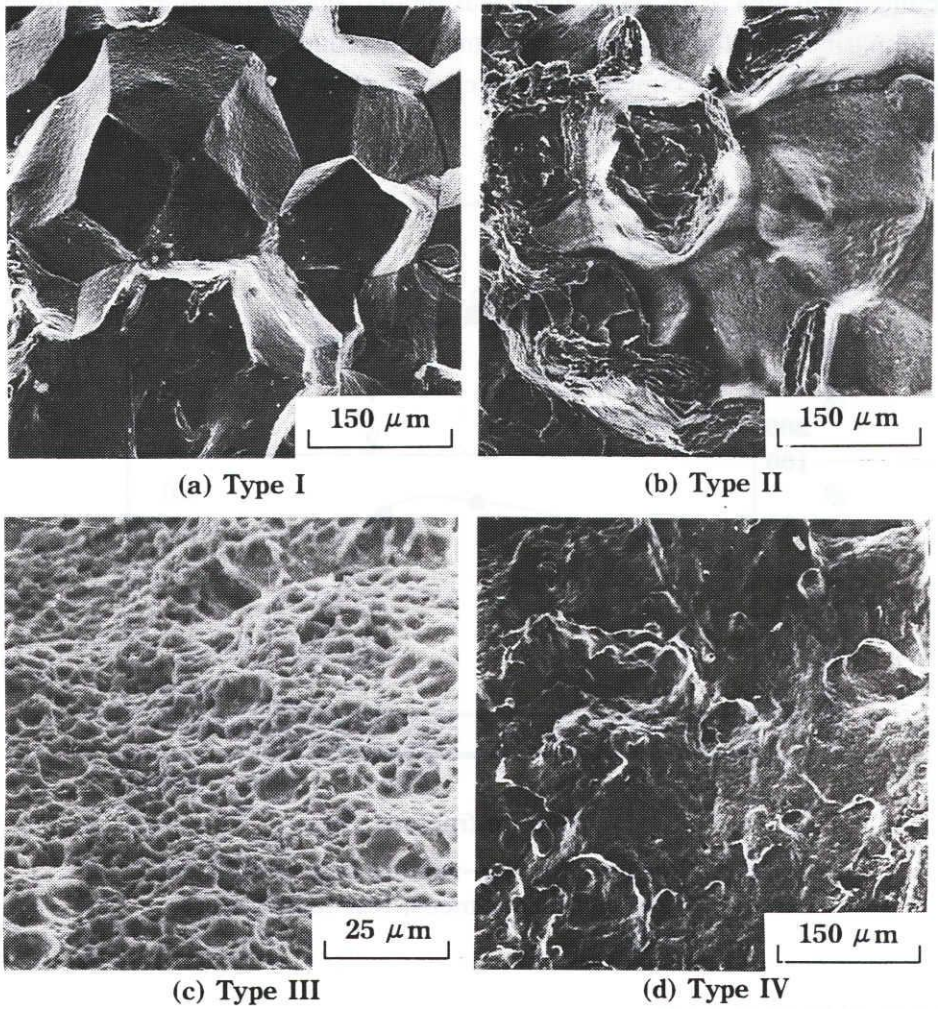

(a) Type I (b) Type II

(c) Type III (d) Type IV

Fig.3 Fracture surface of four typical fracture modes produced by creep–rupture test.

each area was plotted against the time to fracture as shown in Fig.4. The curve attached to the mark ● shows the fraction of type I, and that attached to ○ shows the sum of fractions of type I and II (or type IV, if present). Each width of three (or four) regions divided by the curves shows the fraction of each fracture type. Following changes in the fracture type are recognized with an increasing time to fracture.

At the temperatures 825K and 775K (Fig.4(c) and (d)), the type I appears in the earlier time period. Its fraction becomes maximum at the time t_m and then decreases steeply to zero at the time t_f. In cases of 875K and 850K(Fig.4(a) and (b), its fraction begins to decrease from a very early time period. At the time a little before the t_m, the type II begins to appear its fraction is and increased continuously with an increasing time replacing the type I. The portions in the specimen where the types I and II are produced are restricted in the notch–root under a large stress; they are expanded toward the center of the specimen with decreasing stress.

The type IV (less–ductile, transgranular mode) is observed near the center of the specimen which was fractured after the time t_f' at 875K (Fig.4(a)). The type III (ductile, transgranular mode) is observed around the center portion of all the specimens. Its fraction is large for the short time range but decreases with the lapse of time.

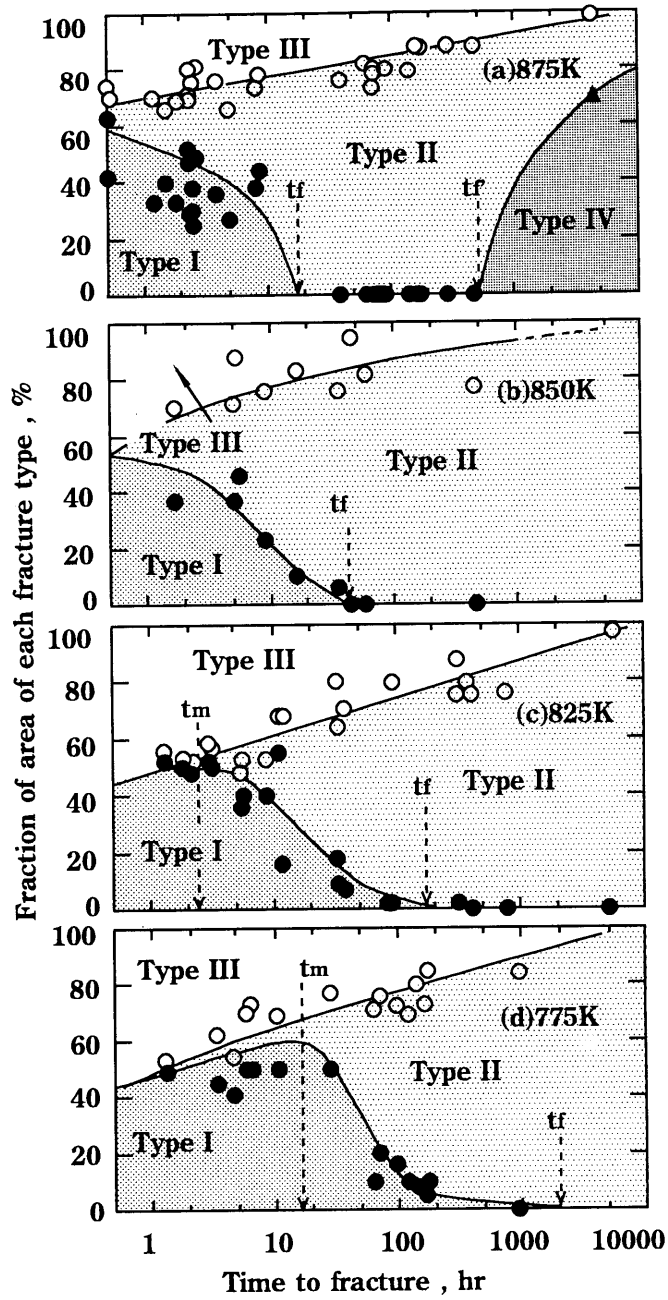

Fig.4 Fractions of areas of fracture types I, II, III and IV; as-welded HAZ specimens.

- ● **fraction of type I**
- ○ **fraction of type I and II or IV**
- ▲ **fraction of type IV**

2.5 Time-temperature-LDCF diagram

The time periods tm, t_f and t_f' (hr) are plotted against the test temperature T (K) as shown in Fig.5. 1/T and log t are taken in the main vertical and horizontal axes of normal spacings; T and t are also shown in the corresponding positions. There are four T-t fields separated by tm, t_f and t_f' lines. The LDCF is classified conveniently into four types (LDCF 1 to 4) according to those fields indicated in Fig.5.

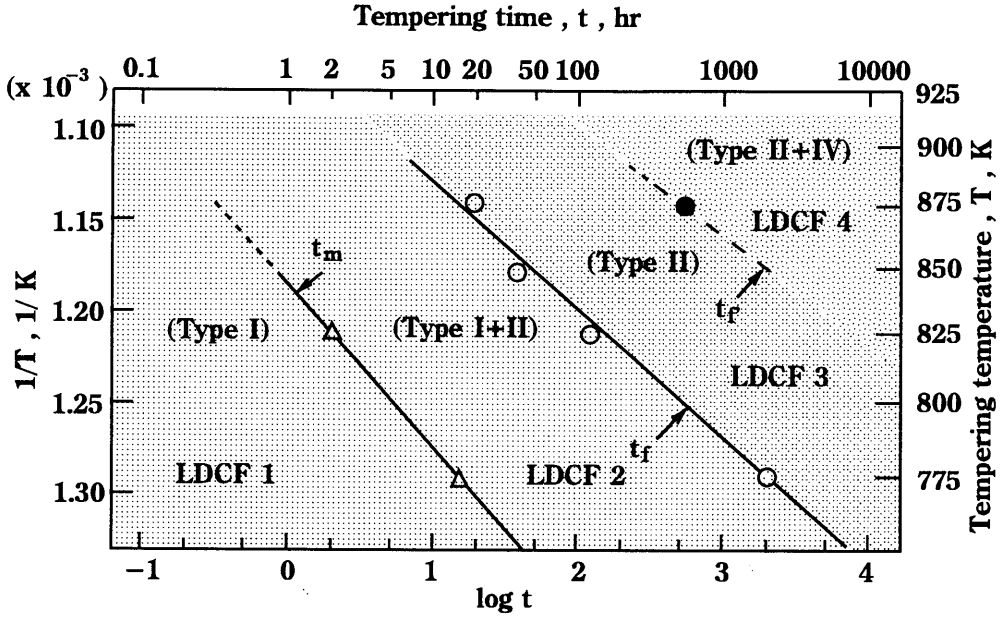

Fig.5 Tempering temperature–time fields where fourth types of LDCF arise in 2 1/4Cr–1Mo steel; Marks show the time periods of: Δ t_m, ○ t_f, ● t_f'.

3. General feature of temper embrittlement

3.1 Experimental procedures

2 1/4Cr–1Mo steel (B) of the chemical composition shown in Table 1 was used. The microstructure of HAZ was reproduced in a steel plate of 7 x 13mm in cross–section by using a weld–thermal–cycle simulator [7]. The simulated HAZ specimens were tempered at 775 to 900K for up to 10000 hours. Charpy impact test below the ambient temperature was made on the half–sized specimen (5 x 10 x 55mm) [7]. The transition curve was drawn for each series of specimens and vTr30, which gave the absorbed energy of 30ft–lb (40.6J), was adopted as the transition temperature.

3.2 Classification of TE

Several types of temper embrittlement arising in the isothermal–tempering process were detected by the following method. Fig.6(a) to (e) show the changes in transition temperature vTr_{30} with an increasing tempering time at the respective tempering temperatures of 775K to 900K. The plots at each temperature are bound by a solid line. The dotted line shows an estimated vTr_{30} of the non–embrittled specimen[6,7].

At 775K, three peaks of vTr_{30} are observed in the solid curve (Fig.6(a)). Each of those peaks will inform each of different types of embrittlement to occur. They are labeled TE 1, TE 2, and TE 3. The time periods at which TE 2 and TE 3 begin to arise will be the points S_2 and S_3, respectively. Those three types of embrittlement are also seen at the temperature of 800K and 825K (Fig.6(b) and (c)). The time periods S_2 and S_3, however, are shortened with a raising temperature.

At 825K, the fourth type of embrittlement (TE 4) appears from the time period S_4 (Fig.6(c)). Three peaks in the curve of 850K will correspond to TE 2, TE 3 and TE 4 (Fig.6(d)). At 875K, the second type disappears at the time period S_D and the specimen becomes the de–embrittled state (DE)[9]. After that, TE 4 begins to appear from the time period S_4 and vTr_{30}

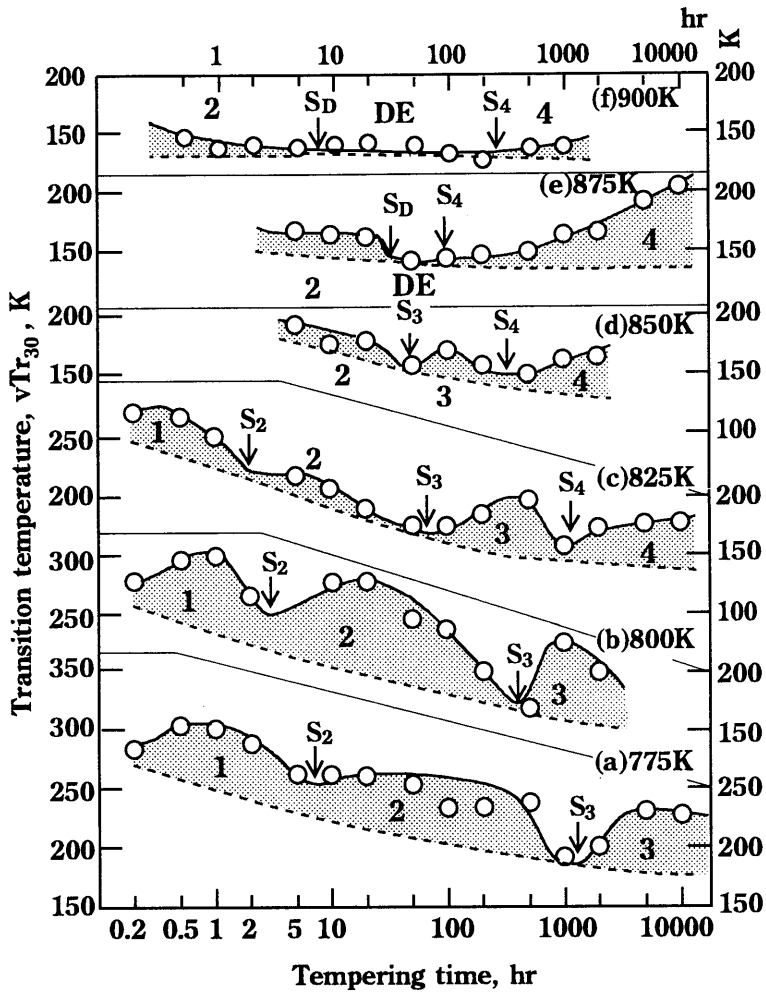

Fig.6 Temper embrittlement observed as the rise of vTr_{30} in each vTr_{30} –tempering time curves.

increases with an increasing time (Fig.6(e)). At 900K, the de-embrittled state continues to occur in a long time range (Fig.6(f)).

3.3 Time-temperature-TE diagram

The time - temperature ranges where the four types of temper embrittlement and the de-embrittled state arise were shown in a diagram of Fig.7 on the basis of the results in Fig.6. 1/T and log t are shown in the main axes, the tempering temperature T (K) and time t (hr) are shown in the corresponding positions of sub-axes. The boundary lines of the regions of the TE 1 to 4 and the de-embrittled state (DE) are drawn referring the time periods S_2 to S_5 and S_D in Fig.6. Fig.7 informs the following facts. (1)TE 3 begins to appear before TE 2 disappears. TE 3 survives after the TE 4 begins to appear. (2)The TE 4 appears in the higher temperature after the de-embrittled state is finished. In the lower temperature, however, it arises in the same time range where the TE 3 continues to occur.

The ultimate temperatures below which TE 3 and TE 4 arises are about 870K and 920K, respectively.

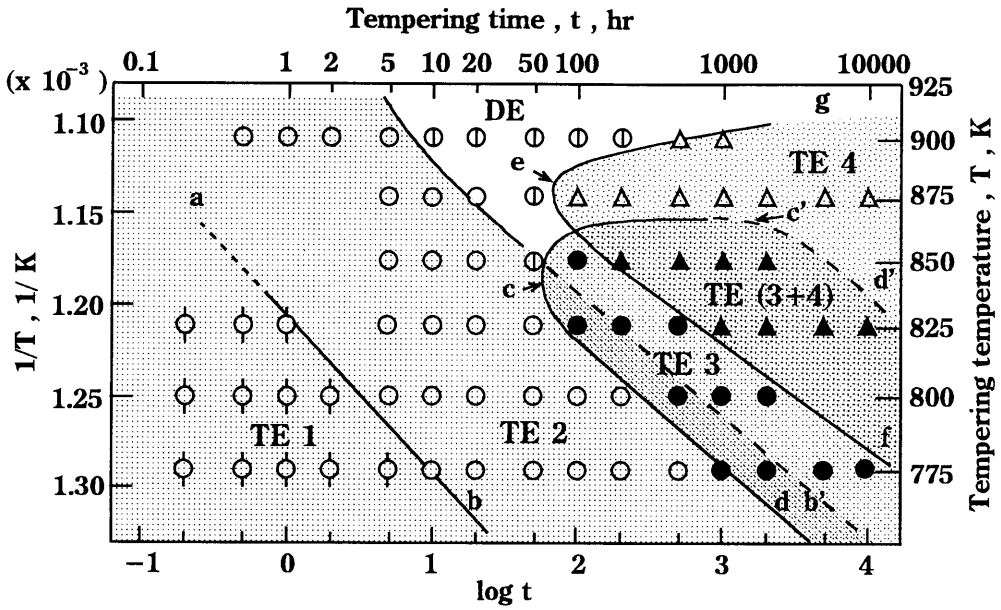

Fig.7 Tempering temperature–time fields where fourth types of temper embrittlement arise in 2 1/4Cr–1Mo steel; Marks show the specimen in the embrittled states of: ϕ first type, ○ second type, ● third type, △ fourth type, ▲ third and fourth types, ⊕ de–embrittled state.

3.4 Fracture types of specimen

The fracture surfaces of impact–tested specimens were observed by an SEM. All the specimens fractured above the vTr30 exhibit a ductile fracture of dimple mode, but those fractured below vTr30 do brittle fractures of two different modes depending on the type of embrittlement as explained below. (1)TE 1 and 2 exhibit the cleavage fracture in ferrite grains. However, the original crack may be initiated at the grain boundaries of prior–austenite, even though they propagate along the cleavage planes (Fig.8(a)). (2)TE 3 exhibits an intergranular fracture. The cracks are initiated and propagated along grain boundaries of prior–austenite (Fig.8(b)). (3)The cleavage fracture was observed in the specimens of TE 4 and the de–embrittled state (Fig.8(c)).

3.5 Time–temperature fields in which LDCF and TE arise

Following facts are recognized by comparing the diagram of LDCF (Fig.5) with that of TE (Fig.7). (1)The time–temperature fields of LDCF 1 and 2, respectively meet very well those of TE 1 and 2. (2)Among the field of LDCF 3, that lower than 860K meets the field of TE 3. (3)The field of LDCF 4 may meet the that of TE 4.

4. Loss of ductility in ferrite grains during tempering

4.1 Effect of carbide particles on loss of ductility

The size of carbide particles was measured by the following method. SEM observations with the magnification of 3000 were made on specimens etched by 3% nital. One photo print of SEM microstructure was selected at random. Carbide particles exhibit a spherical and an elongate shapes; the diameter and the length respectively, were measured for each of these particles.

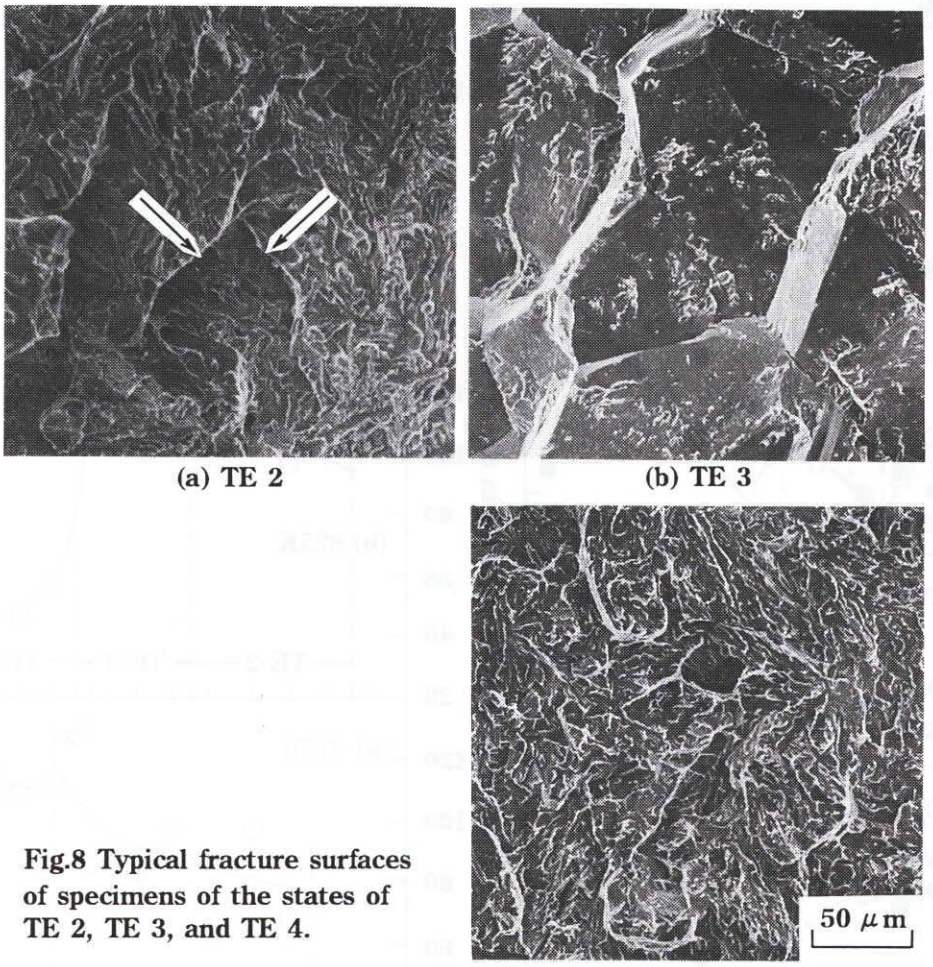

(a) TE 2 (b) TE 3

(c) TE 4

Fig.8 Typical fracture surfaces of specimens of the states of TE 2, TE 3, and TE 4.

Measurements were made separately on the particles in ferrite grains and in grain boundaries of prior-austenite. The number of carbide particles was obtained by the following method. A flame of 5 x 5 um in real size was drawn in an SEM photo print, and the number of particles locating in this flame was counted.

The average size and the number of carbide particles at each tempering temperature are shown in Fig.9 taking the tempering time as the parameter. The time periods at which TE 1 to 4 arise are indicated in the figure. At 775K average sizes of carbide particles decrease with the

lapse of time in the range shorter than S_3, in which TE 1, 2 arise (Fig.9(a)(a')(b) (b')). This result suggests that fine particles of Mo_2C are precipitated replacing coarsened particles of Fe_3C [10].

In the time range in which TE 4 arises, the size of carbide particles increases a little in the time range where TE 3 arises (Fig.9(a)(a')(b)(b')). TE 4 arises at the time when the carbide particles grow very significantly (Fig.9(b)(b')(c)(c')).

4.2 Hardening in ferrite grains during tempering

The hardness of specimen was measured as shown in Fig.10. TE 1 and 2 arise when the secondary hardening, which is brought about by the precipitation of Mo_2C, is observed. The hardness increases a little when TE 3 arises. Hardening does not occur when TE 4 arises; TE 4 will be mainly brought about by the coarsening of carbide particles.

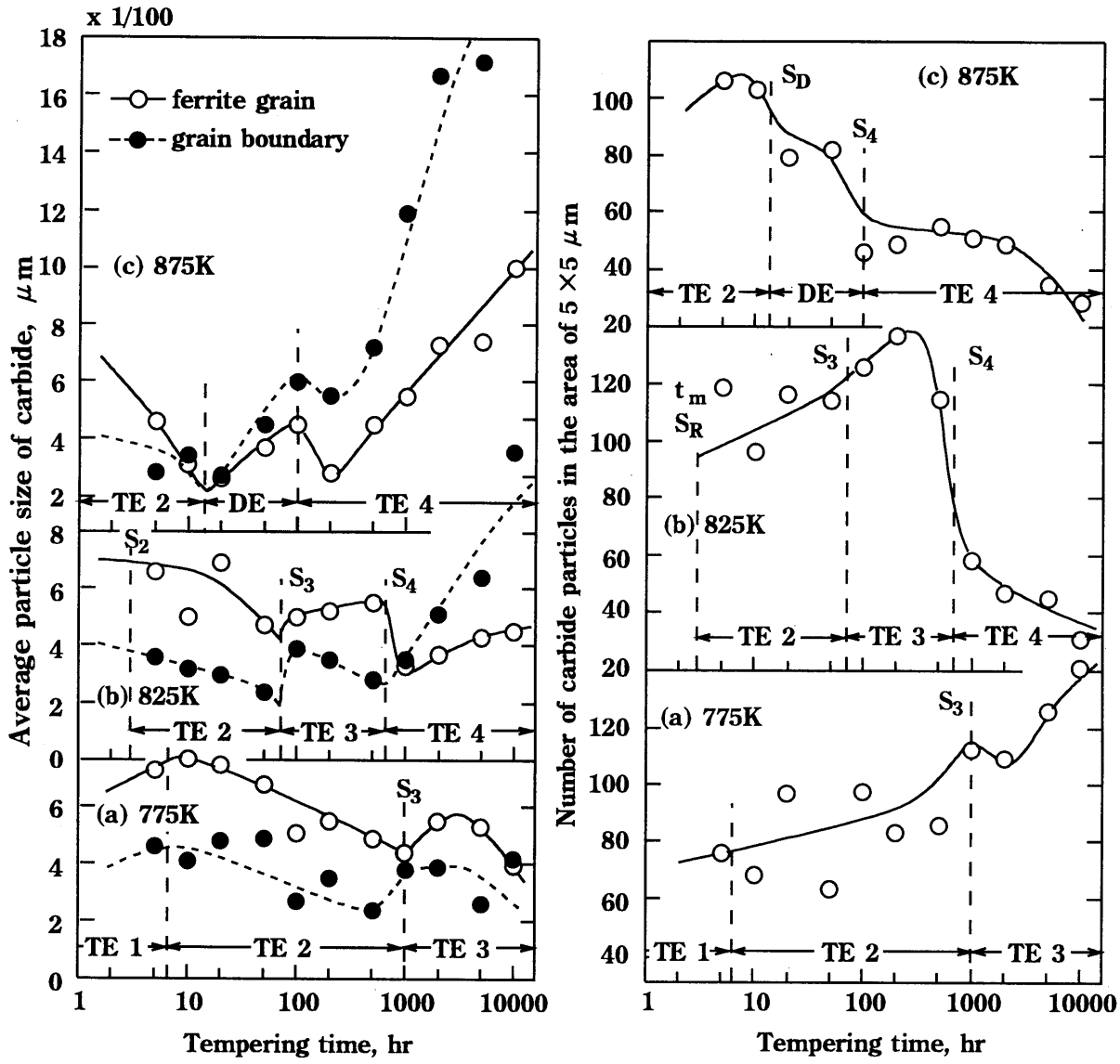

Fig.9 Change in size and number of carbide particles with the lapse of tempering time at 775K to 875K.

5. Weakening in grain boundary during tempering

5.1 Segregation of impurities during short-term tempering

LDCF 1 and 2, which exhibit a typical intergranular fracture, will be induced by the mutual effect of two factors, (1)loss of the ductility of ferrite grains, and (2) weakening of grain boundaries of the prior-austenite which will be brought about by the segregation of impurities. In case of TE 1 and 2, a typical intergranular fracture was not observed, nevertheless, the fractures of Fig.8(a) inform that the cleavage fractures in this case may be initiated at the grain boundaries of, and hence, the segregation of impurity elements may assist TE 1 and 2 to appear.

The mechanism of segregation of impurities is discussed below.

(a) Concept of the authors on the segregation

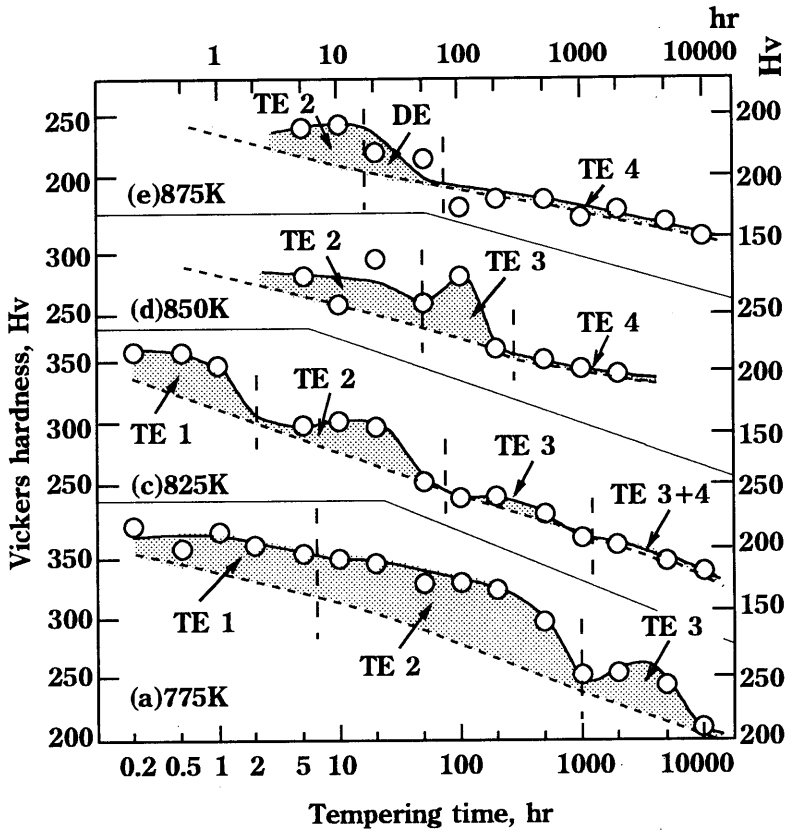

Fig.10 Change of hardness with the lapse of tempering time at 775K to 875K; impact-test specimens.

The authors considered that the segregation of impurities will be originated at the time when a steel is transformed from ferrite to austenite as explained below. (1)The solubility of phosphorus is very large to ferrite but little to austenite, and hence, phosphorus is rejected to the ferrite/austenite interface (the later grain boundary of austenite). After that, phosphorus will be diffused into austenite, if the steel is heated slowly. If it is heated very rapidly as the case of welding, phosphorus cannot be defused and remains at the interface. (2)Phosphorus tends to move away from the grain boundary during the cooling process, but some quantity of it will remain at or near the grain boundary if the cooling rate is so large as the case of welding. (3)Phosphorus will be moved again to the grain boundary during tempering by some micro-structural changes of ferrite matrix, such as the precipitation of Mo_2C.

(b)Experiments on the transforming process under rapid-heating

1/4Cr-1/2Mo steel plate (0.15%C, 0.28%Si, 0.57%Mn, 0.011%P, 0.009%S, 1.09%Cr, 0.55%Mo) was used. The specimen was heated up to the temperature range of 975K to 1425K with the heating rates of 0.05 to 1800K/s, and then water-cooled. In case of the heating rate of 1800K/s, the specimen of 0.5t x5 x7mm was heated by the current flowing through it; in other cases, the specimen of ϕ6 x50mm was heated by the HF induction. The amount of austenite (martensite at room temperature) was measured on the water-quenched specimen by an optical microscope. Summerizing the results of those experiments, the starting and finishing temper-

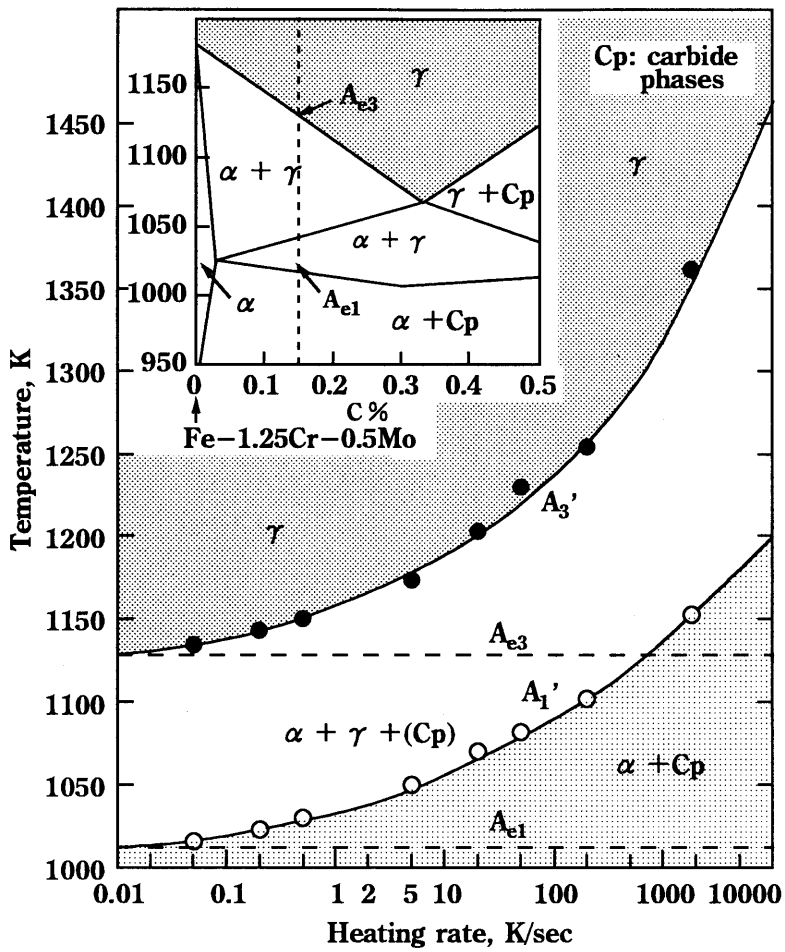

Fig.11 Influence of heating rate on α/γ transformation of 1 1/4Cr−1/2Mo steel

atures of transformation, A_1' and A_3', respectively were decided as shown in Fig.11. The temperatures Ae_1 and Ae_3 in the equilibrium state are shown in the top portion. Fig.11 informs that the temperatures A_1' and A_3', respectively are raised with an increasing logarithm of the heating rate. This tendency is very remarkable in the rage larger than 20K/s.

(c)Experiments on the segregation of impurities

The concentration of phosphorus in grain boundary was semi-quantified by the grain boundary etching method[11]. The specimen was heated up to 1225, 1425 and 1625K with the rates of 10, 100 and 1000K/s by the current flowing through it. The quenched specimen was etched by saturated aqueous solution of picric acid added by a wetting reagent[11] and the depth of etched grain boundary, d was measured as shown in Fig.12. This result informs following facts. (1)Phosphorus is concentrated in the temperature range where the transformation takes place (the range between A_1' and A_3'). (2)The concentration of phosphorus is increased with an increasing heating rate. (3)After the transformation, it is decreased with the rise of temperature. (4)The concentration of phosphorus is decreased with a raising temperature up to A_4 shown in the top of the figure.

Some experiments using the grain boundary etching method have proved that phosphorus was concentrated again in the grain boundary by the short-term tempering by

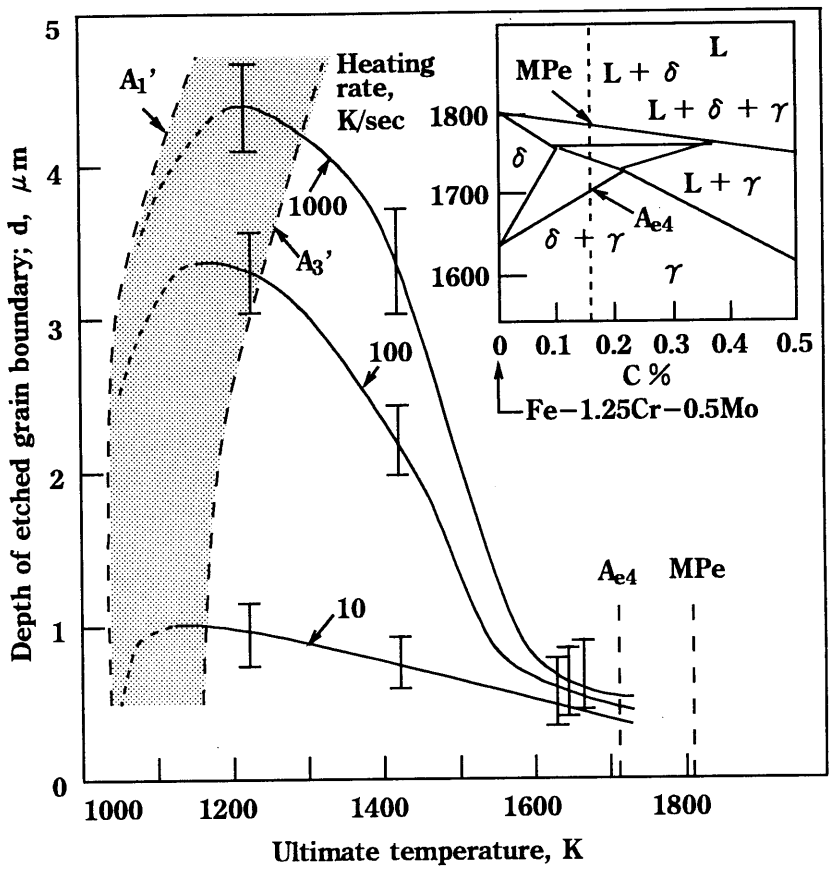

Fig.12 Influence of heating rate and ultimate temperature on the segragation of impurities indicated by the depth of etched grain boundary; 1 1/4Cr–1/2Mo steel

which LDCF 1, 2 and TE 1, arised[11]. This phenomenon may be brought about by the following metallurgical mechanism. (1)The atoms of ferrite-forming element, such as chromium and molybdenum, as well as phosphorus are concentrated at the same sites in the grain boundary. (2)During the short-term tempering, those atoms will move to the interior of ferrite to produce chromium- and molybdenum carbides. At this time, phosphorus atom will take the sites which was occupied by those atoms resulting in the increase of phosphorus concentration in grain boundaries.

5.2 Segregation of impurities during long-term tempering

The segregation of impurities during the long-term tempering was examined by the following method. The specimens suffered from TE 3 was set in an apparatus of Auger electron spectroscopy. An intergranular fracture by an impact blow at the temperature of liquid-nitrogen. Concentrations of elements were analized on several points of the fractured surface. No sign of segregation is seen in the Auger spectra of the cleavage fracture (Fig.13(b)). Segregations of P, Cr, Mo, C, N and O are detected on the intergranular fracture as shown in Fig.13(a). This result suggests following behavior of each group of elements. (a)C and N, which would be

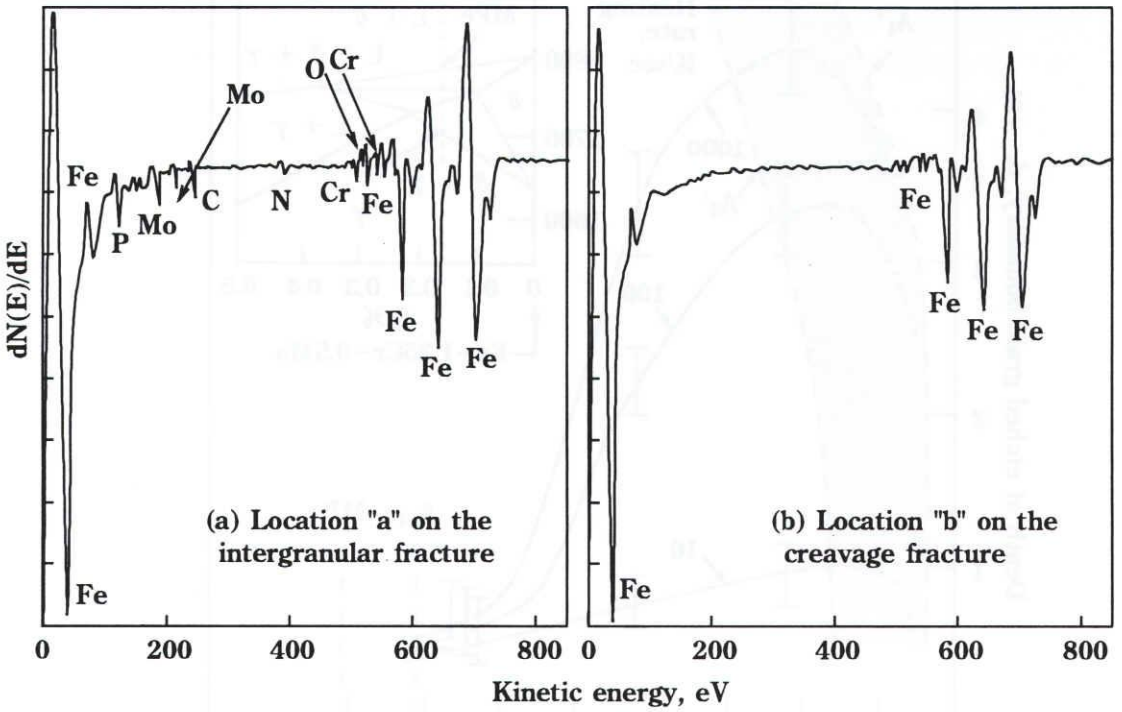

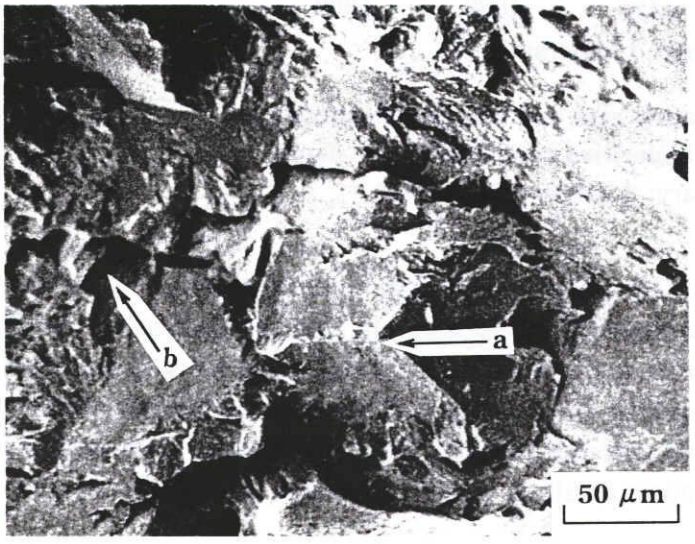

Fig.13 Auger spectra showing the segragation of impurities at grain boundary comparing with that in ferrite grain; specimen tempered at 800K for 1000hr; impurities in bulk steel(B): 0.006P, 0.002S 0.004As, 0.0032N, wt%

dissolved forcibly in ferrite grains by quenching, will be rejected from them and moved to grain boundaries during the long-term tempering. (b)P,Cr and Mo (ferrite-forming elements), which would be segregated originally by welding, will be diffused into ferrite grains during the long-term tempering, but some quantities of them will still remain in the grain boundaries.

6. Conclusions

(1)The LDCF and the TE, respectively are classified into four types, LDCF 1 to 4 and TE 1 to 4 according to the time-temperature range in which each of them arises.

(2)LDCF 1, 2 and TE 1, 2 arise by the short-term tempering. The secondary hardening brought

about by the precipitation of carbide will cause those phenomena. The segregation of phosphorus and some other impurities will assist LDCF 1, 2 to occur.
(3)LDCF 3 and TE 3 arise by the long-term tempering. The segregation of nitrogen and some other impurities will cause those phenomena. The secondary hardening may assist those phenomena to occur.
(4)LDCF 4 and TE 4 arise in the higher-temperature range of tempering. TE 4 will be caused by the coarsening of carbide particles in ferrite grain. LDCF 4 may arise with the same cause as the case of TE 4.

Acknowledgements
The authors wish to thank Mr.H.Wada and Mr.A.Teramoto, the students of Mie University for their cooperations to this research.

References

[1]T.Takamatsu,Y.Otoguro et al.:Effect of metallurgical variables on creep embrittlement of steels, J. Iron and Steel Inst. Japan, 65-7(1979),851-860 (in Japanese).
[2]T.Takamatsu,Y.Otoguro et al.:The effect of postweld heat treatment on creep embrittlement, J. Iron and Steel Inst. Japan , 67-6(1981),774-783 (in Japanese).
[3]T.Ishiguro,Y.Murakami et al.:Metallurgical factors affecting the creep ductility of the HAZ of Cr-Mo pressure vessel steels, J. Iron and Steel Inst. Japan, 70-10(1984), 1421-1428 (in Japanese).
[4]K.Tamaki, H.Kawakami, J.Suzuki, N.Akao, Effect of SR treatment on low ductility creep fracture in HAZ of Cr-Mo steel, Document of Int. Inst. Welding, XI-657/96, (1996, Budapest, Hungary).
[5]F.C.Pickering et al: Material Science and Technology, VCH Verlags, (1992), Vol.7,pp.170-171,461-463.
[6]K.Tamaki, J.Suzuki, H.Kawakami et al: types of temper embrittlement in HAZ of Cr-Mo steel classified by tempering time, IIW Document IX-1745-94, (1994, Beijing, China).
[7]K.Tamaki, J.Suzuki H.Kawakami, K.Tanaka: SR embrittlement and temper embrittlement observed in HAZ of 2 1/4Cr-1Mo steel, Res. Rep. Fac. Mie Univ., vol.20 (1995)
[8]K.Tamaki, H.Kawakami, J.Suzuki et al:Temper embrittlement in HAZ of Cr-Mo steels arising in temperature range of stress relieving, IIW Document IX-1834-96(1996), Budapest, Hungary).
[9]S.Sawada, T.Ohhashi: The de-embrittlement behavior of a temper-embrittled low alloy steel, J. Iron and Steel Inst. Japan , 62-6(1976),644-651 (in Japanese).
[10]K.Tamaki, J.Suzuki et al: Effect of carbides on reheat cracking sensitivity, Trans. Japan Welding Soc., 15-1(1984), 8-16.
[11]K.Tamaki, J.Suzuki, M.Tanaka:Stress-induced phosphorus-segregation and intergranular cracking in welded zone of 1Cr-1/2Mo steel, Res. Rep. Fac. Eng. Mie Univ., Vol.14(1989), 9-22.